Received: 8 May 2018 | Revised: 9 July 2018 | Accepted: 9 July 2018

DOI: 10.1002/er.4178

RESEARCH ARTICLE

WILEY INTERNATIONAL JOURNAL OF ENERGY RESEARCH

Battery hybridization for achieving both high power and high energy densities

Huiseok Kim | Seunghun Jung

School of Mechanical Engineering, Chonnam National University, Gwangju 61186, Republic of Korea

Correspondence
Seunghun Jung, School of Mechanical Engineering, Chonnam National University, 77 Yongbong-ro, Buk-gu, Gwangju 61186, Republic of Korea.
Email: stratus76@hotmail.com

Funding information
Basic Research Lab (BRL), Grant/Award Number: 2015R1A4A1041746; National Research Foundation of Korea; Korea Electric Power Corporation, Grant/Award Numbers: R16EA06 and R17EH01; Resources Core Technology Program, Grant/Award Number: 20142010102930; Korea Institute of Energy Technology Evaluation and Planning

Summary

Instead of developing a new battery to meet required specifications of an automotive battery pack, different batteries can be combined to construct a hybrid battery module to simultaneously achieve both high power and high energy densities in a single system. To investigate the feasibility of battery hybridization concept, a circuit-based hybrid battery model similar to physics-based, blended-electrode model is developed. Our simulation results confirm that the hybrid battery model shows good agreement with physics-based model. Prototype hybrid battery modules consisting of two different lithium-ion batteries are constructed according to various configurations. A computational model representing the constructed hybrid battery module is developed for model validation. Our experimental results show that the capacity and power of a battery module can be controlled by combining different batteries. The computational model of the hybrid battery shows good agreement with experimental results, confirming high fidelity of the proposed model.

KEYWORDS

automotive, hybrid battery, lithium-ion, modeling

1 | INTRODUCTION

Lithium-ion batteries (LiBs) are critical as power source for various types of electric vehicles due to their superior power and energy density compared with previous batteries. However, most LiBs are specially designed and customized to fulfill their specific requirements such as high power for hybrid electric vehicle (HEV) or high energy for battery electric vehicle (BEV) because both high power and high energy densities are difficult to achieve in a single battery.[1] Typically, LiBs for HEVs have thin electrode to achieve high power by reducing internal

Nomenclature:

List of symbols: a_s, active surface area per electrode unit volume (cm^{-1}); c_e, lithium concentration in electrolyte (mol cm^{-3}); c_s, lithium concentration in active particle (mol cm^{-3}); C, capacitance (μF); D_e, lithium diffusion coefficient in electrolyte ($cm^2\ s^{-1}$); D_s, lithium diffusion coefficient in active particle ($cm^2\ s^{-1}$); E, open-circuit voltage (V); E_{act}, activation energy; F, Faraday constant (96 487 C mol^{-1}); i, current density (A cm^{-2}); i_0, exchange current density (A cm^{-2}); I, current (A); j, volumetric current density (A cm^{-3}); k, reaction coefficient; L, thickness (cm); r, radial coordinate (cm); R, resistance (Ω); R_u, universal gas constant (8.314 $J{\cdot}mol^{-1}{\cdot}K^{-1}$); t, time (s); t_+^o, transference number of lithium ion with respect to the velocity of solvent; T, temperature (K); x, thickness coordinate (cm)

Greek letters: α_a, α_c, anodic and cathodic transfer coefficient for an electrode reaction; ε, porosity; ϕ_e, electrolyte phase potential (V); ϕ_s, solid phase potential (V); η, surface overpotential of an electrode reaction (V); κ, ionic conductivity (S cm^{-1}); κ_D, diffusive conductivity of a species (A cm^{-1}); σ, electronic conductivity (S cm^{-1})

Superscripts and subscripts: eff, effective; E, high energy cell (E-cell); i, ith member; j, jth member; P, high power cell (P-cell); rxn, reaction

resistance although they lack in energy storage. In contrast, high energy batteries for BEVs with thick electrode to store large amounts of active material could suffer from voltage loss or lithium-metal plating problem under high C-rate condition. These explain the trade-off between high power and high energy.

To achieve high power and high energy densities in LiBs, several studies have focused on the performance improvement of LiB components such as electrolyte,[2] membrane,[3] and active materials.[4] However, a lot of time and effort are required to develop a new material that can support both power and energy requirements simultaneously as the new material must demonstrate performance, reliability, and compatibility with other components. Instead of developing a new material, a combination of two or more existing materials or components in a single system could be considered.

To exploit each active materials, two or more active materials can be blended into a single electrode called a "blended electrode." Myung et al[5] have experimentally investigated electrochemical characteristics of a positive electrode by blending $Li_{1.1}Mn_{1.9}O_4$ and $LiNi_{0.8}Co_{0.15}Al_{0.05}O_2$. Whitacre et al[6] have studied the performance of a composite LiB cathode by changing the configuration of composite electrodes. Gomadam et al[7] have predicted the voltage-capacity behavior of a primary LiB with a blended cathode constructed with high energy active material (CF_x) and high power active material (SVO) through a mathematical approach. Jung[8] has developed an equilibrium model to rapidly predict the equilibrium voltage profile of a blended electrode in addition to a physics-based model (PBM) to predict the dynamic behavior of LiBs with blended electrodes for various configurations. Although his equilibrium model is useful and effective for quick evaluation of the capacity and voltage profile of a blended electrode, it lacks the capability of dynamic simulation. On the other hand, PBM is unsuitable for battery management system (BMS) because it lacks real-time calculation capability that is necessary for BMS. Furthermore, subsequent computational studies on blended electrode of a LiB have been reported.[9-14] These works mainly follow physics-based approach focusing on transport phenomena, which requires heavy computational cost. Li et al[13] have developed a reduced order model of LiB with blended cathode. Yet their model is complex and unsuitable for BMS applications. Jung et al[14] have developed a two-dimensional blended-electrode model focusing on the effect of electrode morphologies.

CSIRO Energy Technology has introduced an ultrabattery to promote power capability with longer life than conventional lead-acid batteries.[15,16] The ultrabattery has a single positive electrode and a hybridized anode consisting of a parallel combination of a carbon layer and a lead layer. The carbon layer works as a supercapacitor that boosts power capability of the battery. However, the ultrabattery still has limited power and energy density compared with LiBs because it is a minor modification of conventional lead-acid battery. Similarly, LiB electrodes can be hybridized by combining capacitors in a single system. Cericola et al[17,18] have examined the pros and cons of battery-capacitor system for serial/parallel combinations and reported that serial combination of battery and capacitor does not provide any benefit. However, parallel combination can improve the specific power by reducing internal resistance. Instead of internally combining the electrode and capacitor in a single battery, a battery can be externally connected to other components such as a supercapacitor,[19,20] fuel cell,[21-26] or even with photovoltaic cell[27,28] to construct a hybridized battery system.

The present study aims to improve both power and energy densities of LiB by externally hybridizing battery module with two different types of LiBs for automotive applications. To achieve this goal, we first developed a computational model to accurately capture the performance of externally hybridized battery modules. After conducting a feasibility study with the developed computational model, a prototype of the hybridized battery module was actually constructed and tested. Finally, the internal behavior and characteristics of the hybridized battery module were analyzed with the computational model.

2 | COMPUTATIONAL

2.1 | Derivation of hybridized battery model

An electrochemical system such as LiB can be simply expressed as an equivalent circuit model (ECM).[29-31] A hybrid battery module that consists of two cells connected in parallel can be expressed as an ECM as shown in Figure 1A. The present study used an ECM with a single resistance/capacitor pair (RC pair) rather than two RC pairs to avoid the complexity in parameter extraction from experimental data. Cell voltage of each cell is expressed as

$$\begin{aligned} V_{\text{cell,A}} &= E_{\text{A}} - V_{\text{A0}} - V_{\text{A1}} = E_{\text{A}} - I_{\text{A}}R_{\text{A0}} - V_{\text{A1}} \\ V_{\text{cell,B}} &= E_{\text{B}} - V_{\text{B0}} - V_{\text{B1}} = E_{\text{B}} - I_{\text{B}}R_{\text{B0}} - V_{\text{B1}}. \end{aligned} \tag{1}$$

Currents are calculated as follows:

$$\begin{cases} I = I_{\text{A}} + I_{\text{B}} \\ I_{\text{A}} = I_{\text{A1}} + I_{\text{A2}} \\ I_{\text{B}} = I_{\text{B1}} + I_{\text{B2}} \end{cases} \quad \text{where} \quad \begin{cases} I_{\text{A1}} = \dfrac{V_{\text{A1}}}{R_{\text{A1}}}, I_{\text{A2}} = C_{\text{A1}}\dfrac{dV_{\text{A1}}}{dt} \\ I_{\text{B1}} = \dfrac{V_{\text{B1}}}{R_{\text{B1}}}, I_{\text{B2}} = C_{\text{B1}}\dfrac{dV_{\text{B1}}}{dt} \end{cases}. \tag{2}$$

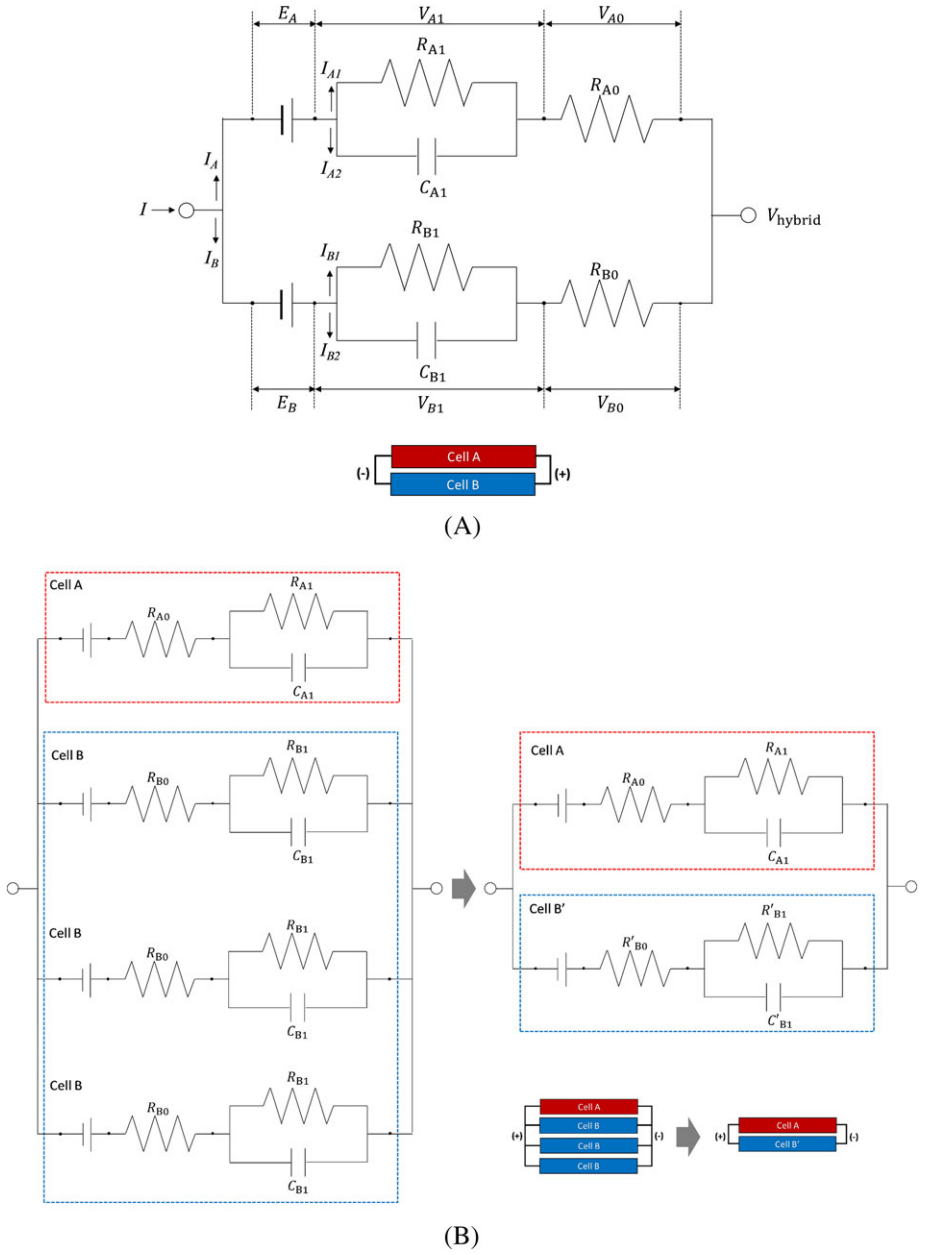

FIGURE 1 A, Equivalent circuit of a hybrid battery module with two different lithium-ion cells. B, Equivalent circuit of a hybrid battery module with four lithium-ion cells in parallel connection [Colour figure can be viewed at wileyonlinelibrary.com]

The following two state equations are derived from Equations (1) and (2).

$$\begin{aligned}\frac{dV_{A1}}{dt} &= -\frac{1}{R_{A1}C_{A1}}V_{A1} + \frac{1}{C_{A1}}I_A \\ \frac{dV_{A2}}{dt} &= -\frac{1}{R_{B1}C_{B1}}V_{B1} + \frac{1}{C_{B1}}I_B\end{aligned} \tag{3}$$

To calculate current distribution to each cell of the hybrid battery module, input current (I) is considered to be distributed to each cell by two factors: (1) serial resistance ratio and (2) potential difference. Current load part that is inversely proportional to immediate resistance is represented as follows:

$$I_A^* = \left(\frac{R_{B0}}{R_{A0}+R_{B0}}\right)I, \quad I_B^* = \left(\frac{R_{A0}}{R_{A0}+R_{B0}}\right)I. \tag{4}$$

In addition, we defined current controlled by potential difference between two cells as follows:

$$I_A^{**} = \frac{1}{R_{A0}+R_{B0}}(V_B - V_A), \quad I_B^{**} = \frac{1}{R_{A0}+R_{B0}}(V_A - V_B)$$
$$\text{where } V_A = E_A - V_{A1} \text{ and } V_B = E_B - V_{B1}. \tag{5}$$

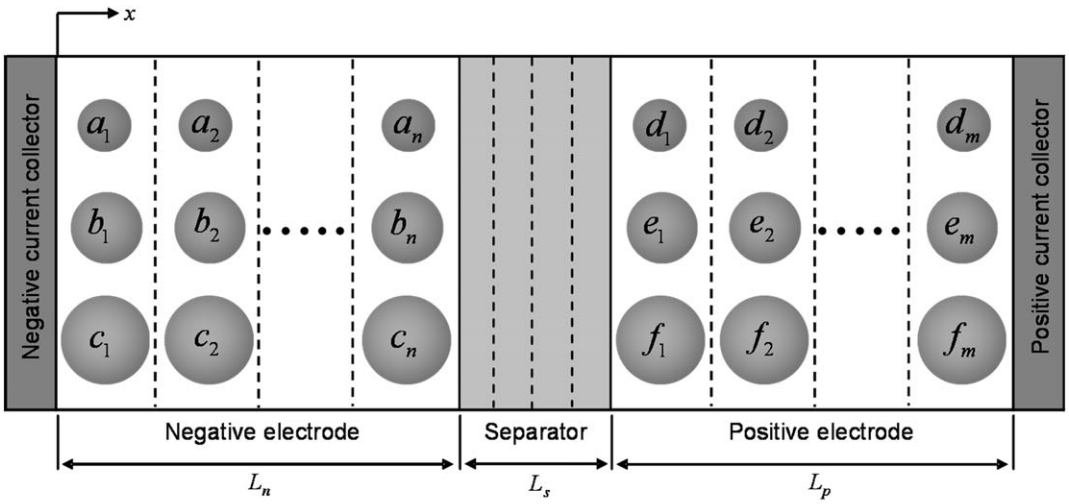

(A)

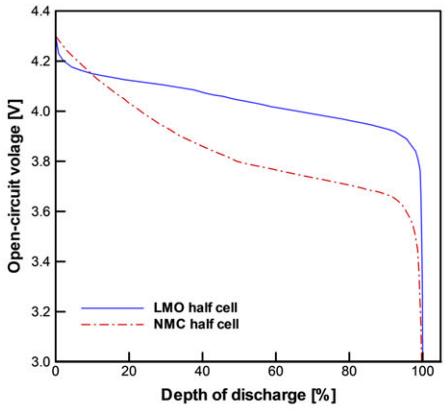

(B)

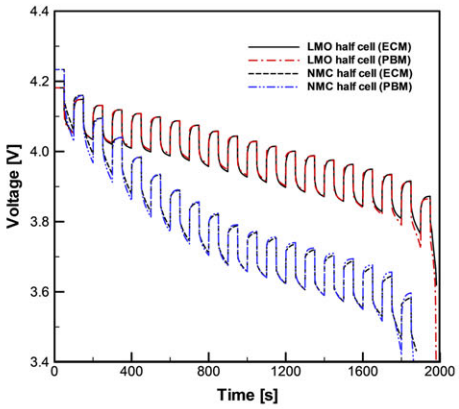

(C)

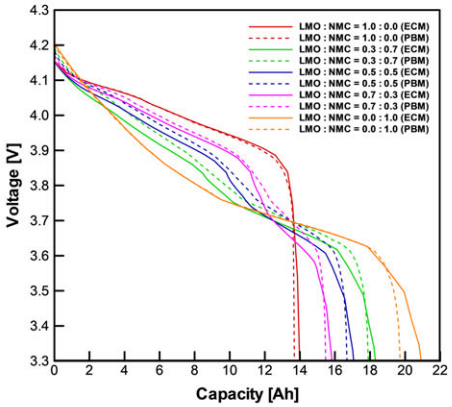

(D)

FIGURE 2 A, Computation domain of the physics-based, blended-electrode model.[8] B, Open-circuit voltages of lithium manganese oxide (LMO) half-cell and lithium nickel cobalt manganese oxide (NMC) half-cell. C, Direct current impulse response test data generated by physics-based model (PBM) of LMO half-cell and NMC half-cell. D, Comparison of discharging voltage profiles of blended-electrodes generated by PBM and equivalent circuit model according to the blending ratio of LMO and NMC [Colour figure can be viewed at wileyonlinelibrary.com]

TABLE 1 Governing equations of physics-based, blended-electrode model[8]

Description	Conservation Equation	Boundary Condition
Electrolyte phase potential	$\frac{\partial}{\partial x}\left(\kappa^{\text{eff}}\frac{\partial \phi_e}{\partial x}\right)+\frac{\partial}{\partial x}\left(\kappa_D^{\text{eff}}\frac{\partial}{\partial x}\ln c_e\right)=-j$	$\left.\frac{\partial \phi_e}{\partial x}\right\|_{x=0}=\left.\frac{\partial \phi_e}{\partial x}\right\|_{x=L}=0$
Solid phase potential	$\frac{\partial}{\partial x}\left(\sigma^{\text{eff}}\frac{\partial \phi_s}{\partial x}\right)=j$	$-\sigma_-^{\text{eff}}\left.\frac{\partial \phi_s}{\partial x}\right\|_{x=0}=\sigma_+^{\text{eff}}\left.\frac{\partial \phi_s}{\partial x}\right\|_{x=L}=i$ $-\sigma_-^{\text{eff}}\left.\frac{\partial \phi_s}{\partial x}\right\|_{x=L_n}=\sigma_+^{\text{eff}}\left.\frac{\partial \phi_s}{\partial x}\right\|_{x=L_{n+s}}=0$
Lithium concentration in electrolyte	$\frac{\partial(\varepsilon_e c_e)}{\partial t}=\frac{\partial}{\partial x}\left(D_e^{\text{eff}}\frac{\partial c_e}{\partial x}\right)+\frac{1-t_+^o}{F}j$	$\left.\frac{\partial c_e}{\partial x}\right\|_{x=0}=\left.\frac{\partial c_e}{\partial x}\right\|_{x=L}=0$
Lithium concentration in active particle	$\frac{\partial c_s}{\partial t}=D_s\frac{\partial^2 c_s}{\partial r^2}+\frac{2D_s\partial c_s}{r\ \partial r}$	$c_s=c_{s,0}$ at $t=0$ $D_s\frac{\partial c_s}{\partial r}=0$ at $r=0$ $D_s\frac{\partial c_s}{\partial r}=\frac{j}{F}$ on particle surface
Primary electrochemical reaction of particle i	$j_{\text{rxn,i}}=a_s i_0\left\{\exp\left(\frac{\alpha_a F}{R_u T}\eta\right)-\exp\left(-\frac{\alpha_c F}{R_u T}\eta\right)\right\}$	$\eta=\phi_s-\phi_e-E$
Interactive reaction between particle i and j	$j_{ij}=k_{ij}(a_{s,ij}i_{0,ij})\Delta E_{ij}\cdot\exp\left\{\frac{E_{\text{act}}}{R_u}\left(\frac{1}{T_{\text{ref}}}-\frac{1}{T}\right)\right\}$	$\Delta E_{ij}=E_i-E_j$
Charge conservation (when particles 1 and 2 are blended)	$j=\sum_{i=1} j_i=j_1+j_2$	$j_1=j_{\text{rxn},1}+j_{12}$ $j_2=j_{\text{rxn},2}+j_{21}$

TABLE 2 Cell dimensions and material properties of physics-based, blended-electrode model

Parameter	Value	Unit	Note
Radius of NMC particle	4.5	μm	
Radius of LMO particle	7.5	μm	
Li-ion diffusivity in NMC particle	5.5×10^{-10}	$cm^2\ s^{-1}$	8
Li-ion diffusivity in LMO particle	2.5×10^{-9}	$cm^2\ s^{-1}$	8
Thickness of electrode	62/60/ 58.5/ 57/55	μm	Case 1/2/3/4/5
Thickness of separator	16	μm	
Porosity of electrode	0.25		
Porosity of separator	0.37		
Transference number	0.363		
Faraday's constant (F)	96,487	$C\ Mol^{-1}$	
Li-ion diffusivity in electrolyte	2.5×10^{-6}	$cm^2\ s^{-1}$	8
Average Li-ion conc in electrolyte	1.0	M	
Electronic conductivity in electrode	0.062	$S\ cm^{-1}$	8

TABLE 3 Simulation cases of the blended-electrode model

	LMO Loading, mg cm^{-2}	NMC Loading, mg cm^{-2}	Cell Width, cm	Cell Length, cm	No. of Electrodes	Cell Capacity, Ah
Case 1	16.0	0.0	15	18	32	14.0
Case 2	11.2	4.8	15	18	32	16.0
Case 3	8.0	8.0	15	18	32	17.5
Case 4	4.8	11.2	15	18	32	18.8
Case 5	0.0	16.0	15	18	32	21.0

Therefore, net current distributed to each cell is

$$I_A = I_A^* + I_A^{**}, \quad I_B = I_B^* + I_B^{**} \quad . \tag{6}$$

The hybrid battery voltage becomes

$$V_{\text{hybrid}} = \left(\frac{R_{B0}}{R_{A0}+R_{B0}}\right)V_A + \left(\frac{R_{A0}}{R_{A0}+R_{B0}}\right)V_B - \left(\frac{R_{A0}R_{B0}}{R_{A0}+R_{B0}}\right)I. \tag{7}$$

This model can be extended to hybrid batteries with more than two constituting cells. Figure 1B shows a hybrid battery module with four lithium-ion cells. Because three of them are the same (cell B), they can be combined to be an imaginary cell (cell B′) as follows:

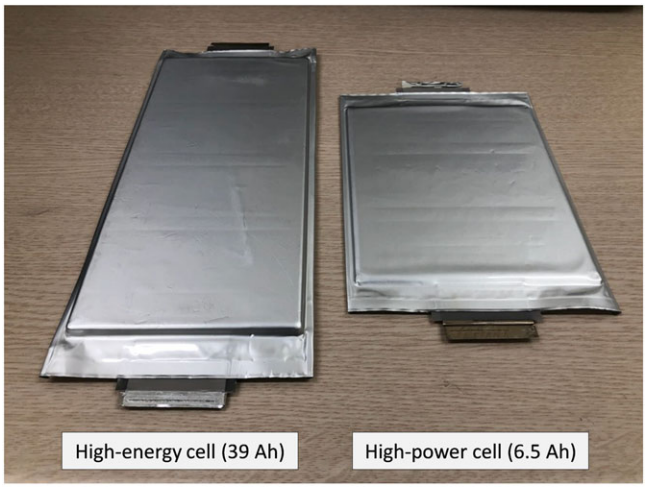

(A)

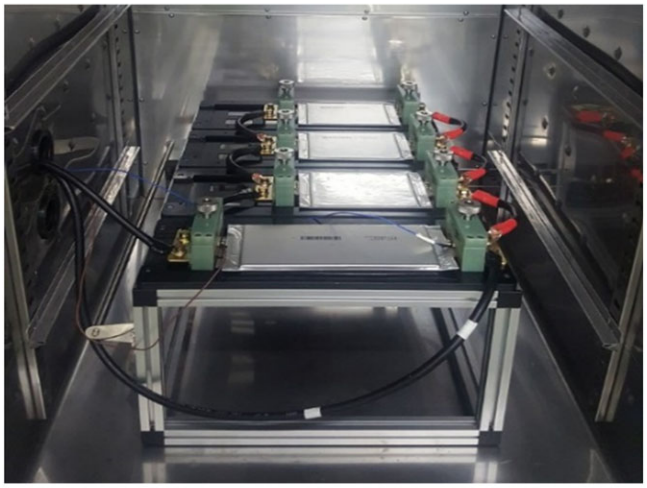

(B)

FIGURE 3 A, High-energy cell (E-cell, 39 Ah) and high-power cell (P-cell, 6.5 Ah) used in the present study. B, Experimental apparatus for testing battery hybridization (1E3P case in the figure) [Colour figure can be viewed at wileyonlinelibrary.com]

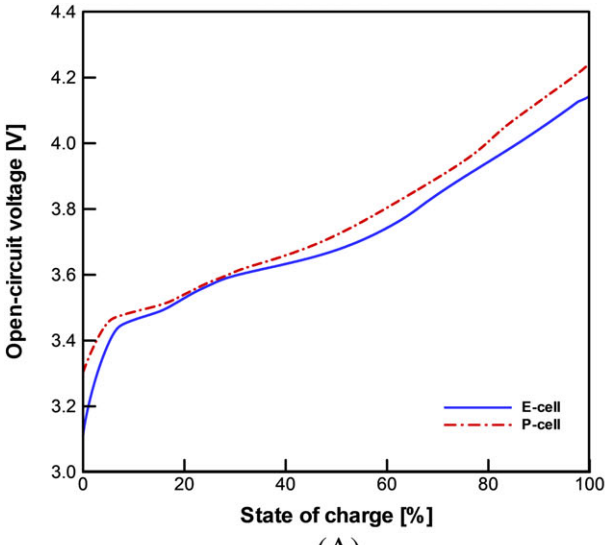

(A)

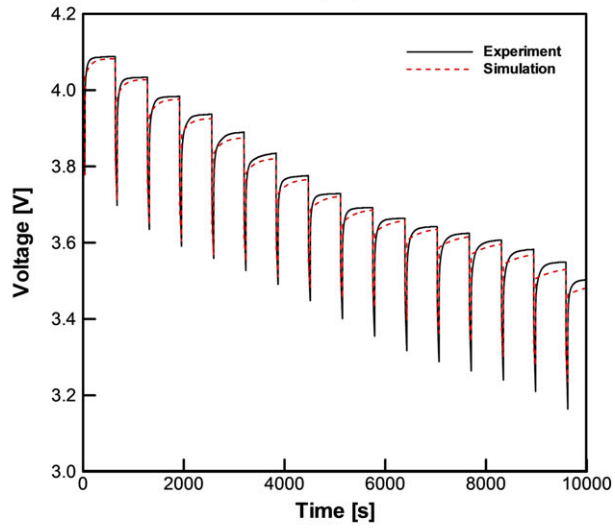

(B)

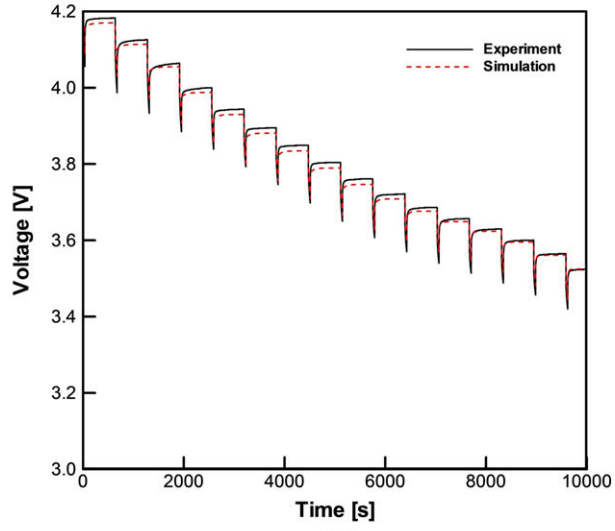

(C)

FIGURE 4 A, Open-circuit voltages of P-cell and E-cell. B, Direct current impulse response (DCIR) result of E-cell. C, DCIR result of P-cell [Colour figure can be viewed at wileyonlinelibrary.com]

$$R'_{B0} = \frac{1}{n}R_{B0}, R'_{B1} = \frac{1}{n}R_{B1}, C'_{B1} = nC_{B1} \quad (n = 3 \text{ for Figure 1C}) \tag{8}$$

Therefore, this battery combination follows the same logic as the model shown in Figure 1A. To complete the model, ECM parameters such as E, R_0, R_1, and C_1 must be obtained for each of the constituting cell from experimental data. The model is implemented into MATLAB/Simulink and solved iteratively.

2.2 | Comparison with physics-based model

The basic concept of the physics-based blended electrode model is that neighboring different active particles will try to form an electrical potential equilibrium by conducting an internal charge/discharge against each other. Therefore, the concept of battery hybridization through external connection of several different batteries is considered to be similar to that of the blended-electrode system proposed by Jung.[8] For this reason, physics-based blended-electrode model was used to verify the fidelity of the hybrid battery model in the present study.

Computational domain of the PBM is presented in Figure 2A. Each electrode may consist of several different types of active materials such as lithium manganese oxide (LMO), lithium nickel cobalt manganese oxide (NMC), and lithium iron phosphate (LFP) in the positive electrode. Negative electrode in Figure 2A is not used here because half-cells are simulated for model validation. Governing equations and model parameters of the PBM are summarized in Tables 1 and 2, respectively. Detailed introduction to the blended-electrode model can be found elsewhere.[8] Five half-cell models consisting of LMO and NMC are generated according to the blending ratio of LMO and NMC shown in Table 3. Each cell has the same dimension and number of electrodes but different active material loading amounts.

Distinct profile shapes of open-circuit voltage (OCV) are compared between LMO and NMC as shown in Figure 2B. When LMO and NMC are blended in an electrode, a blended OCV profile is expected. To extract ECM parameters of LMO half-cell (case 1) and NMC half-cell (case 5), direct current impulse response (DCIR) tests were computationally simulated using a PBM, as shown in Figure 2C. The ECMs of blended electrodes (cases 2, 3, and 4) were generated by combining ECMs of cases 1 and 5 according to the blending ratio, not by extracting model parameters from the PBM of blended electrodes.

Discharging voltage profiles of the ECM are compared with those of the PBM according to various blending ratios of LMO and NMC as shown in Figure 2D. Results confirmed that the present hybrid battery model was fundamentally equivalent to the blended-electrode model. Therefore, it is expected that the hybrid battery model can predict the performance of a hybrid battery module with various battery combinations without conducting an experiment for each combination.

3 | EXPERIMENTAL

3.1 | Experimental setup

Two types of LiBs for automotive applications were prepared for battery hybridization. One was a high-energy

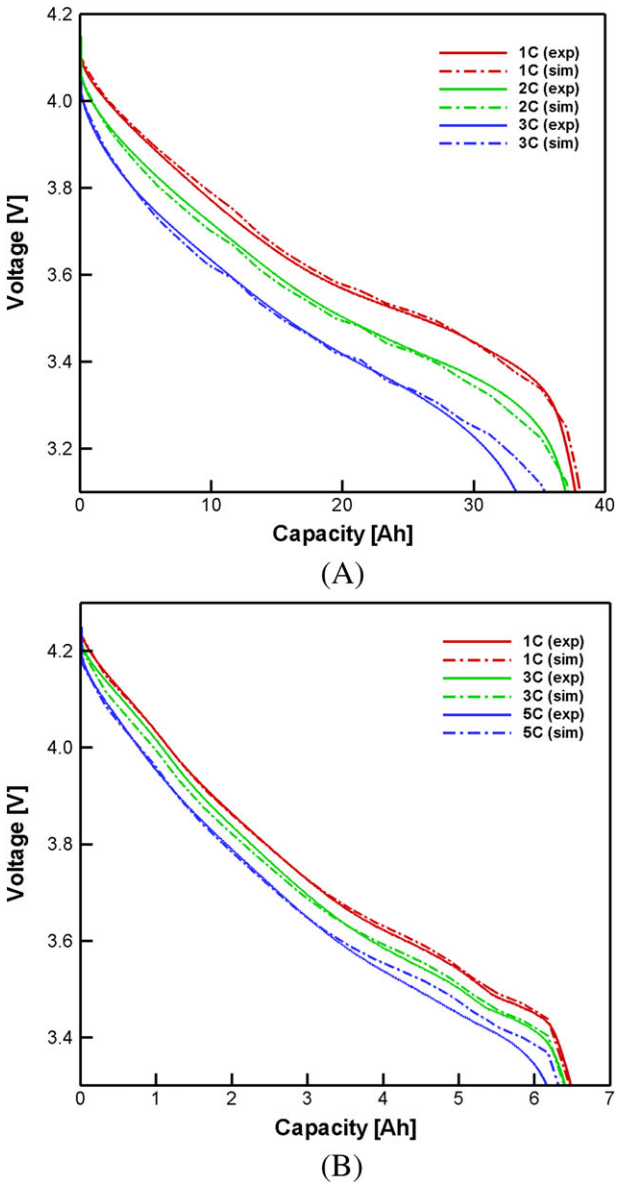

FIGURE 5 Comparison of discharging performance between E-cell and P-cell [Colour figure can be viewed at wileyonlinelibrary.com]

cell (E-cell) for BEVs, which had 39-Ah nominal capacity. The other was a high-power cell (P-cell) for HEV, which had 6.5-Ah nominal capacity (see Figure 3A). To evaluate various combinations of these cells, a specially designed jig was prepared as shown in Figure 3B. The hybrid battery module was placed in an environmental chamber and tested with a battery tester.

3.2 | Unit cell characterization for model construction

Before constructing the hybrid battery model, an E-cell and a P-cell were characterized to extract the model parameters such as voltage curve, resistance, and capacitance. First, OCV curves were determined by average

TABLE 4 Cell combinations of the hybrid battery module

	No. of E-cell	No. of P-cell	Lower Cutoff Voltage, V	Upper Cutoff Voltage, V	Cell Capacity, Ah
Case 1 (0E1P)	0	1	3.3	4.25	6.5
Case 2 (1E0P)	1	0	3.1	4.15	39.0
Case 3 (1E1P)	1	1	3.3	4.15	43.5
Case 4 (1E2P)	1	2	3.3	4.15	49.5
Case 5 (1E3P)	1	3	3.3	4.15	55.5

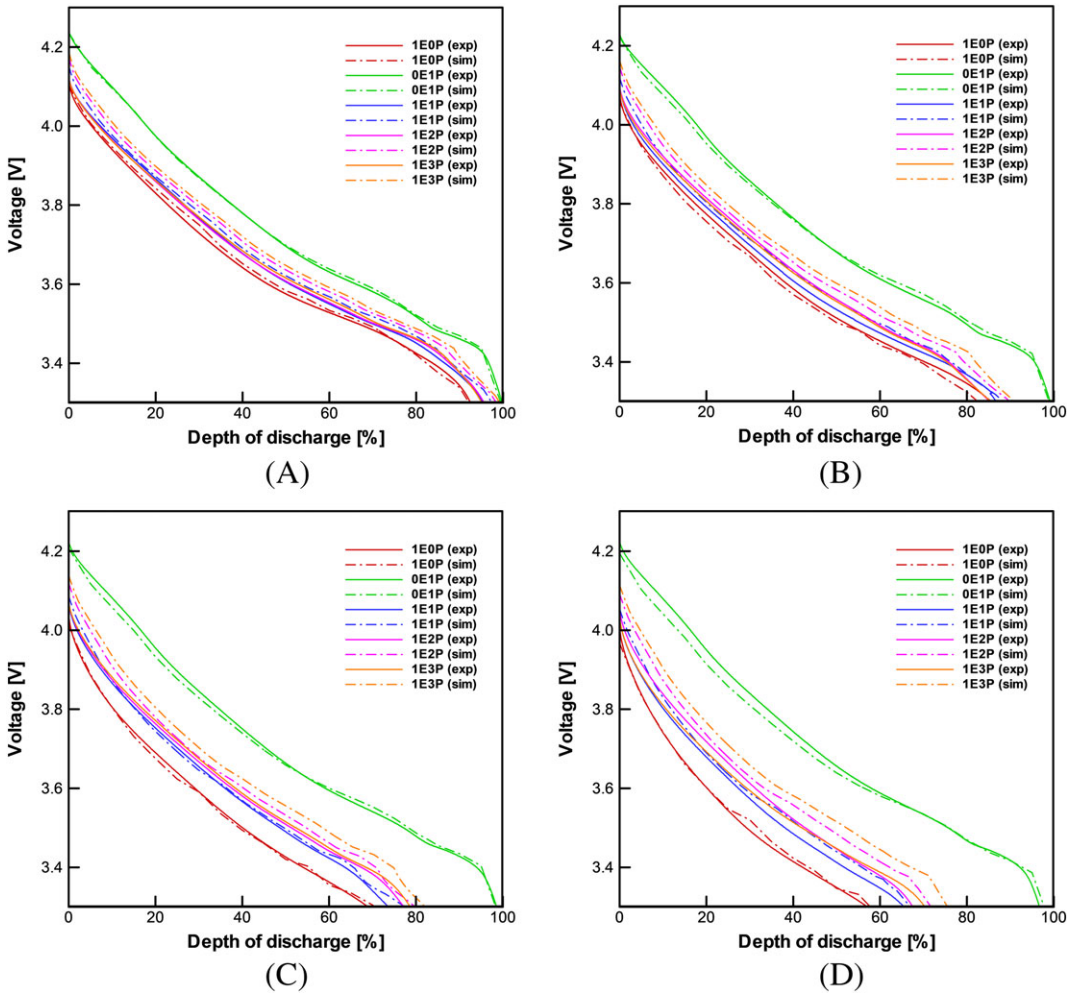

FIGURE 6 Discharging voltage profiles of hybrid batteries under A, 1C condition; B, 2C condition; C, 3C condition; and D, 4C condition [Colour figure can be viewed at wileyonlinelibrary.com]

values of charging and discharging voltage profiles under a very low C-rate condition as shown in Figure 4A. Next, DCIR test was conducted to evaluate R_0, R_1, and C_1 values as shown in Figure 4B,C. Figure 5 compares simulation result and experimental data of the discharging performance of E-cell and P-cell. Results showed that simulation data agreed well with experimental data and that P-cell had better power capability than E-cell.

3.3 | Performance of hybrid battery module

To investigate the effect of battery hybridization, five combinations of constituting cells were chosen as listed in Table 4. Because nominal voltage windows of E-cell (3.1-4.15 V) and P-cell (3.3-4.25 V) were not perfectly aligned, the voltage window of the hybrid battery was adjusted to be between 3.3 and 4.15 V to avoid battery damage from overcharging or overdischarging. Because of this adjustment, nominal capacity of the hybrid battery was slightly lower than the capacity sum of E-cell and P-cell.

The discharging performance of each hybrid battery module was evaluated. Results are shown in Figure 6. Compared with case 2 (1E0P), addition of P-cells to E-cell (1E1P ➔1E2P ➔1E3P) gradually improved the power capability of the battery module. Overall, the computational model predicted the actual performance of hybrid batteries relatively well, although some deviations were observed under high C-rate condition. This deviation could have been mitigated if the model was improved by adopting two RC pairs instead of one RC pair.

3.4 | Load distribution in hybrid battery module

When a hybrid battery module is discharged by the constant-current mode, the current load is distributed to each constituting cell (E-cell and P-cell). This current distribution can be analyzed using the hybrid battery model, as shown in Figure 7. Although a constant-current load was applied to the hybrid battery module, distributed current to each cell continuously varied because of several reasons such as internal resistance, potential difference,

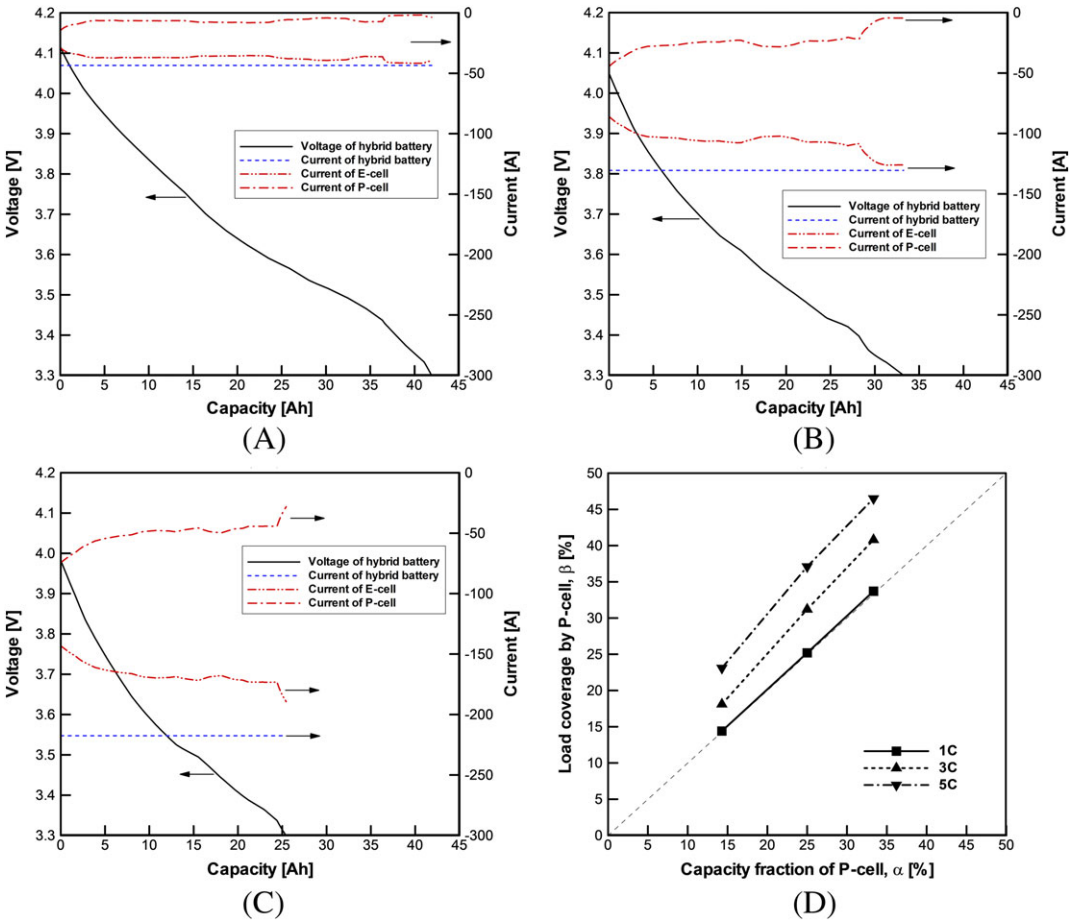

FIGURE 7 Current distribution to P-cell and E-cell in 1E1P battery module for A, 1C; B, 3C; C, 5C discharging; and D, load coverage by P-cell according to capacity fraction of P-cell in a hybrid battery (capacity fraction 15% for 1E1P, capacity fraction 25% for 1E2P, and capacity fraction 33% for 1E3P) [Colour figure can be viewed at wileyonlinelibrary.com]

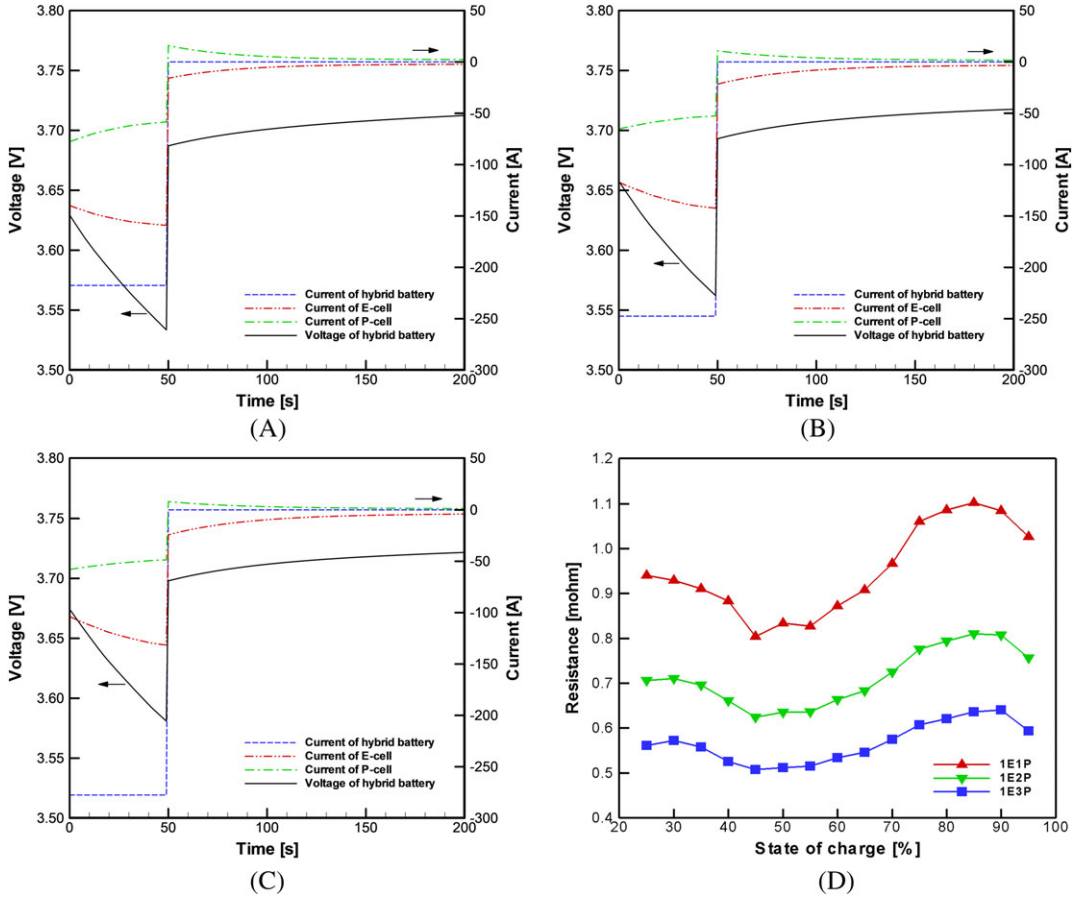

FIGURE 8 Direct-current response of A, 1E1P; B, 1E2P; C, 1E3P; and D, internal resistance of hybrid batteries (5C discharging for 3 min, then rested for 10 min at each point) [Colour figure can be viewed at wileyonlinelibrary.com]

and state of charge (SOC). Although P-cell had limited capacity compared with E-cell, P-cell operated until the end of the discharging, meaning P-cell behaved as a buffer. When C-rate was low, the load coverage ratio of P-cell was almost the same as the capacity fraction of P-cell in the hybrid battery module, meaning that P-cell had little influence on power improvement of the hybrid battery module under low C-rate condition.

$$\alpha = \text{Capacity fraction of P-cell} = \frac{capa_{\mathrm{P}}}{capa_{\mathrm{E}} + capa_{\mathrm{P}}} \times 100\ (\%)$$

$$\beta = \text{Load coverage ratio of P-cell} = \frac{\int I_{\mathrm{P}} dt}{\int I dt} \times 100\ (\%) \tag{9}$$

When the hybrid battery module undergoes a continuous charging or discharging, the load coverage by P-cell gradually decreases owing to limited capacity of P-cell compared with that of E-cell. Therefore, it will be more effective to introduce some relaxation time to recover SOC of the P-cell rather than a continuous operation without any relaxation time. This will be further discussed in Section 3.5.

Figure 7D shows the effect of P-cell on load coverage of a hybrid battery module according to capacity fraction of P-cell. The load coverage of P-cell is almost proportional to the capacity fraction of P-cell under low C-rate (1C) condition. However, it is clear that the load coverage of P-cell is increased and the power capability of the hybrid battery module is improved under high C-rate condition (3C and 5C).

3.5 | Dynamic behavior of hybrid battery module

To investigate the dynamic behavior of the hybrid battery module, a high current test was simulated using the hybrid battery model. Results are shown in Figure 8. First, a high-current discharge (5C) was conducted for 50 seconds. Then the battery module was set to rest (150 s) so that the battery module response could be examined. Initially, the SOC was set at 66% for each hybrid battery module. As the capacity fraction of P-cell increased (1E1P ➔1E2P ➔1E3P), current load to E-cell mitigated and voltage loss decreased. When a high load was applied to the hybrid battery module, P-

cell could spread over a large portion of the load, resulting in a power boost ($0 < t < 50$ s). Immediately after the external load was released, an internal current flowed from E-cell to P-cell in the hybrid battery module ($50 < t < 200$ s). In other words, E-cell charged P-cell owing to the dynamic potential difference between cells to restore potential equilibrium. This helped P-cell restore buffer capability. The relaxation time to restore the buffer capability of P-cell was around 2 minutes as shown in Figure 8A, although this time would change according to C-rate condition, temperature, active material types, SOC, and so on. The relaxation time is considered to be mostly dependent of Li-ion diffusion speed of the active particle in E-cell, which is much slower than that of P-cell.

The internal resistance of the hybrid battery modules is acquired by conducting a high C-rate discharge/rest for every 5% of SOC as shown in Figure 8D. Compared with 1E1P case, 1E2P and 1E3P cases had 25% and 40% lower internal resistance, respectively, by combining P-cells with E-cell. Evidently, the power capability of the hybrid battery module was improved owing to lowered internal resistance.

4 | CONCLUSION

A computational and experimental study of battery hybridization to achieve both high power and high energy was conducted for the first time in this study. First, a circuit-based computational model of the hybrid battery was developed and validated with a PBM, which showed good agreement. This result indicates that the present circuit-based hybrid battery model could be used as a core model of BMS for batteries with blended-electrodes such as NMC/LMO, NMC/LFP, and so on. Second, actual hybrid battery modules were constructed and tested by combining high-energy cell (E-cell) and high-power cells (P-cell). We observed that P-cell improved power capability of a hybrid battery module by reducing the internal resistance, especially under high C-rate condition. The hybrid battery model predicted the performance of the actual hybrid battery module with high accuracy. Furthermore, we found that P-cell required some relaxation time to recover its capacity from E-cell immediately after an intervention in a strong current load. By connecting P-cell to E-cell to construct a hybrid battery module, the internal resistance of the battery module was significantly reduced, resulting in high power capability of the hybrid battery module.

Because P-cell would distribute strong load to E-cell that is vulnerable to high power operations, such hybrid battery concept is expected to delay battery degradation. Proper voltage window of the hybrid battery module also needs to be identified to maximize the effectiveness of the battery hybridization.

ACKNOWLEDGEMENTS

This work was financially supported by the Basic Research Lab (BRL) program (No. 2015R1A4A1041746) funded by the National Research Foundation of Korea, the Korea Electric Power Corporation (R16EA06 and R17EH01), and the Resources Core Technology Program (No. 20142010102930) of the Korea Institute of Energy Technology Evaluation and Planning (KETEP) from the Ministry of Trade, Industry and Energy, Republic of Korea.

ORCID

Seunghun Jung http://orcid.org/0000-0003-0762-8063

REFERENCES

1. Takami N, Inagaki H, Tatebayashi Y, Saruwatari H, Honda K, Equsa S. High-power and long-life lithium-ion batteries using lithium titanium oxide anode for automotive and stationary power applications. *J Power Sources*. 2013;244:469-475.
2. Chen Z, Lu WQ, Liu J, Amine K. LiPF6/LiBOB blend salt electrolyte for high-power lithium-ion batteries. *Electrochim. Acta Theriol*. 2006;51(16):3322-3326.
3. Shin WK, Yoo JH, Kim DW. Surface-modified separators prepared with conductive polymer and aluminum fluoride for lithium-ion batteries. *J Power Sources*. 2015;279:737-744.
4. Zhang SS, Foster D, Read J. A high energy density lithium/sulfur–oxygen hybrid battery. *J Power Sources*. 2010;195(11):3684-3688.
5. Myung ST, Cho MH, Hong HT, Kang TH, Kim CS. Electrochemical evaluation of mixed oxide electrode for Li-ion secondary batteries: Li1.1Mn1.9O4 and LiNi0.8Co0.15Al0.05O2. *J Power Sources*. 2005;146(1-2):222-225.
6. Whitacre JF, Zaghib K, West WC, Ratnakumar BV. Dual active material composite cathode structures for Li-ion batteries. *J Power Sources*. 2008;177(2):528-536.
7. Gomadam PM, Merritt DR, Scott ER, Schmidt CL, Skarstad PM, Weidner JW. Modeling Li/CF[sub x]-SVO hybrid-cathode batteries. *J Electrochem Soc*. 2007;154(11):A1058.
8. Jung S. Mathematical model of lithium-ion batteries with blended-electrode system. *J Power Sources*. 2014;264:184-194.
9. Basu S, Patil RS, Ramachandran S, et al. Non-isothermal electrochemical model for lithium-ion cells with composite cathodes. *J Power Sources*. 2015;283:132-150.
10. Mao Z, Farkhondeh M, Pritzker M, Fowler M, Chen Z, Safari M. Model-based prediction of composition of an unknown blended lithium-ion battery cathode. *J Electrochem Soc*. 2015;162(4):A716-A721.

11. Mao Z, Farkhondeh M, Pritzker M, Fowler M, Chen Z. Dynamics of a blended lithium-ion battery electrode during galvanostatic intermittent titration technique. *Electrochim. Acta Theriol*. 2016;222(20):1741-1750.
12. Lu T, Luo Y, Zhang Y, Luo W, Yan L, Xie J. Degradation analysis of a lithium-ion battery with a blended electrode. *J Electrochem Soc*. 2017;164(2):A295-A303.
13. Li X, Choe SY, Joe WT. A reduced order electrochemical and thermal model for a pouch type lithium ion polymer battery with LiNi x Mn y Co 1−x−y O 2 /LiFePO 4 blended cathode. *J Power Sources*. 2015;294:545-555.
14. Jung S. Computational study about the effect of electrode morphology on the performance of lithium-ion batteries. *Int J Energy Res*. 2016;40(8):1073-1084.
15. Lam LT, Louey R. Development of ultra-battery for hybrid-electric vehicle applications. *J Power Sources*. 2006;158(2):1140-1148.
16. Cooper A, Furakawa J, Lam L, Kellaway M. The UltraBattery—a new battery design for a new beginning in hybrid electric vehicle energy storage. *J Power Sources*. 2009;188(2):642-649.
17. Cericola D, Novák P, Wokaun A, Kötz R. Hybridization of electrochemical capacitors and rechargeable batteries: an experimental analysis of the different possible approaches utilizing activated carbon, Li4Ti5O12 and LiMn2O4. *J Power Sources*. 2011;196(23):10305-10313.
18. Cericola D, Kötz R. Hybridization of rechargeable batteries and electrochemical capacitors: principles and limits. *Electrochim. Acta Theriol*. 2012;72:1-17.
19. Miller JM, The 7th Int. Conference on Power Electronics; 2007; 16.
20. Wang Y, Zhang X, Liu C, Pan R, Chen Z. Multi-timescale power and energy assessment of lithium-ion battery and supercapacitor hybrid system using extended Kalman filter. *J Power Sources*. 2018;389:93-105.
21. Andreasen SJ, Ashworth L, Remón INM, Kær SK. Directly connected series coupled HTPEM fuel cell stacks to a Li-ion battery DC bus for a fuel cell electrical vehicle. *Int J Hydrogen Energy*. 2008;33(23):7137-7145.
22. Zhang X, Mi CC, Masrur A, Daniszewski D. Wavelet-transform-based power management of hybrid vehicles with multiple on-board energy sources including fuel cell, battery and ultracapacitor. *J Power Sources*. 2008;185(2):1533-1543.
23. Kojima T, Ishizu T, Horiba T, Yoshikawa M. Development of lithium-ion battery for fuel cell hybrid electric vehicle application. *J Power Sources*. 2009;189(1):859-863.
24. Bubna P, Brunner D, Gangloff JJ Jr, Advani SG, Prasad AK. Analysis, operation and maintenance of a fuel cell/battery series-hybrid bus for urban transit applications. *J Power Sources*. 2010;195(12):3939-3949.
25. Fadel A, Zhou B. An experimental and analytical comparison study of power management methodologies of fuel cell–battery hybrid vehicles. *J Power Sources*. 2011;196(6):3271-3279.
26. Andaloro L, Arista A, Agnello G, Napoli G, Sergi F, Antonucci V. Study and design of a hybrid electric vehicle (Lithium Batteries-PEM FC). *Int J Hydrogen Energy*. 2017;42(5):3166-3184.
27. Joos S, Weißhar B, Bessler WG. Passive hybridization of a photovoltaic module with lithium-ion battery cells: A model-based analysis. *J Power Sources*. 2017;248:201.
28. Wu W, Hu W, Teng Y, Qian S, Cheng R. Optimal integration of a hybrid solar-battery power source into smart home nanogrid with plug-in electric vehicle. *J Power Sources*. 2017;363:277-283.
29. Verburgge MW, Conell RS. Electrochemical and thermal characterization of battery modules commensurate with electric vehicle integration. *J Electrochem Soc*. 2002;149(1):A45.
30. Liaw BY, Nagasubramanian G, Jungst RG, Doughty DH. Modeling of lithium ion cells—a simple equivalent-circuit model approach. *Solid State Ion*. 2004;175:835-839.
31. Jung S, Kang D. Multi-dimensional modeling of large-scale lithium-ion batteries. *J Power Sources*. 2014;248:498-509.

How to cite this article: Kim H, Jung S. Battery hybridization for achieving both high power and high energy densities. *Int J Energy Res*. 2018;1–12. https://doi.org/10.1002/er.4178